Green Chemistry

PAPER

View Article Online
View Journal | View Issue

Cite this: *Green Chem.*, 2020, **22**, 6855

Tuning selectivity of CO_2 hydrogenation by modulating the strong metal–support interaction over Ir/TiO_2 catalysts†

Yaru Zhang,[a,b] Zhen Zhang,[c] Xiaofeng Yang,[a] Ruifeng Wang,[a] Hongmin Duan,[a] Zheng Shen,[a] Lin Li,[a] Yang Su,[a] Runze Yang,[c] Yongping Zhang,[c] Xiong Su,*[a] Yanqiang Huang *[a] and Tao Zhang[d]

Exploration of highly selective catalysts for CO_2 hydrogenation remains a great challenge since the reduction of CO_2 over the supported metal catalysts may give rise to various products in response to the modulation of the chemical state of active sites. Herein, by varying the pretreatment temperature of iridium/titanium oxide (Ir/TiO_2) catalysts, the selectivity of CO_2 hydrogenation from CH_4 to sole production of CO can be finely tuned. The change of product selectivity is achieved in such a way that the selectivity greatly depend on the formation of a reduced TiO_x overlayer around Ir nanoparticles (NPs) as originated from the strong metal–support interaction (SMSI). With only a weak reduction treatment, the exposed Ir NPs without a TiO_x coating promote CH_4 production exclusively. After the catalyst undergoes a high temperature reduction, the evolution of the TiO_x coating over Ir NPs shows a preference for CO production with an inhibition of further methanation. This study not only provides insights into the regulation of CO_2 hydrogenation by SMSI, but also serves as an effective approach to tuning other catalytic processes.

Received 6th July 2020,
Accepted 15th September 2020

DOI: 10.1039/d0gc02302g

rsc.li/greenchem

Introduction

The ever-increasing threats of global warming and dramatic climate changes have drawn increasing attention in recent years. Carbon dioxide (CO_2), as a major greenhouse gas, is being blamed for the ecological troubles. On the other hand, CO_2 also serves as an ideal C1 source, and catalytic CO_2 hydrogenation offers an effective strategy for the transformation of CO_2 into high value-added chemicals[1–3] and fuels[4–6] by which the global carbon cycle can be sustained simultaneously.

Catalytic CO_2 hydrogenation at atmospheric pressure usually consists of two competitive processes over the supported Group VIII metal catalysts. One is direct CO_2 methanation, known as the Sabatier reaction,[7–9] and the other is CO_2 hydrogenation to carbon monoxide (CO), known as the reverse water–gas shift (RWGS) reaction.[10–12] Exploration of highly selective catalysts with the aim of acquiring desired products for each process still remains a great challenge. So far, enormous efforts have been devoted to tuning the selectivity of CO_2 hydrogenation, including tuning the metal particle size,[13–15] modifying the chemical state, changing the support type[16,17] or crystal phase,[18] and adding promoters.[17,19] Despite these developments, intrinsic factors that govern the product selectivity remain less understood. As previously reported by Christopher *et al.*, the product selectivity of CO_2 hydrogenation greatly depended on the active sites, that is, atomically dispersed isolated rhodium (Rh) sites selected for CO production and Rh nanoparticles (NPs) selected for CO_2 methanation.[20] Our group has reported recently that, when decreasing the coordination number of metal sites to one, CO production was significantly enhanced by the inhibition of carbonyl dissociation and simultaneous facilitation of CO desorption.[21] On the other hand, researchers have found that it was the chemical state of Ir species, rather than the coordination of metals, nanoparticles or single-atoms, that played a more important role in controlling product selectivity.[22]

Reducible oxides like titanium oxide (TiO_2) and cerium oxide (CeO_2) are widely used as supports in CO_2 hydrogenation, as they give adequate assistance for CO_2 activation.[23–25] More importantly, strong metal–support interactions (SMSI)

[a]*CAS Key Laboratory of Science and Technology on Applied Catalysis, Dalian Institute of Chemical Physics, Chinese Academy of Sciences, Dalian 116023, China. E-mail: suxiong@dicp.ac.cn, yqhuang@dicp.ac.cn*
[b]*University of Chinese Academy of Sciences, Beijing 100049, China*
[c]*China Astronaut Research and Training Center, Beijing 100094, China*
[d]*State Key Laboratory of Catalysis, Dalian Institute of Chemical Physics, Chinese Academy of Sciences, Dalian 116023, China*

†Electronic supplementary information (ESI) available: Additional characterizations of Ir/TiO_2 catalysts. See DOI: 10.1039/d0gc02302g

on reducible oxide-supported metal catalysts occur,[26–28] where H_2 and CO chemisorption can be suppressed and will further influence the catalytic CO_2 hydrogenation processes. The intrinsic role of SMSI in tuning the selectivity of CO_2 hydrogenation is worth studying in depth.

In this study, we succeeded in fabricating a highly dispersed Ir/TiO_2 catalyst with resistance to agglomeration even when treated at high temperatures (up to 700 °C). By varying the reduction temperature, SMSI on Ir/TiO_2 are modulated, which further plays a crucial role in tuning the product selectivity. With a weak reduction treatment at low temperatures (lower than 300 °C), metallic Ir NPs expose on the catalyst surface and promote CH_4 production exclusively. After the catalyst undergoes a high temperature reduction, Ir NPs are entirely encapsulated by reduced TiO_x species, which show a preference for CO production with an inhibition of further methanation. With this knowledge, we show that highly selective CO_2 hydrogenation processes toward either of the two products can be achieved by tailoring the SMSI over the supported metal catalysts.

Results and discussion

Catalytic performance of Ir/TiO_2-x catalysts

A series of Ir/TiO_2 catalysts, with a 2.45 wt% Ir loading as detected by inductively coupled plasma optical emission spectroscopy (ICP-OES), were pretreated at different temperatures and were denoted as Ir/TiO_2-x, where x refers to the reduction temperature (x = 200–700 °C). The catalytic CO_2 hydrogenation tests of these catalysts were performed at 280 °C under atmospheric pressure. As shown in Fig. 1, the series of Ir/TiO_2-x catalysts show a similar catalytic activity as reflected by the reaction rate, whereas a divergence in product selectivity from CH_4 to CO is observed with an increase in the reduction temperature from 200 to 700 °C. Samples pretreated at temperatures lower than 300 °C exhibited complete methanation of CO_2 conversion. An improved selectivity toward CO was observed as the reduction temperature increased, and a further increase of reduction temperature beyond 600 °C led to complete CO formation.

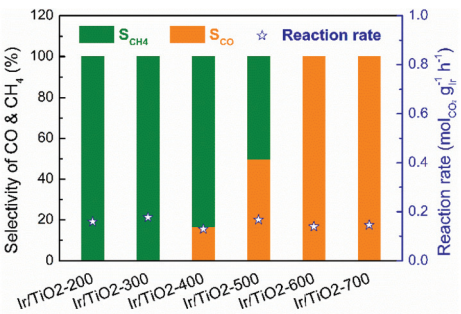

Fig. 1 Catalytic performance of the series of Ir/TiO_2-x catalysts for CO_2 hydrogenation reactions. Reaction conditions: 280 °C, 0.1 MPa, space velocity = 9000 mL h^{-1} g_{cat}^{-1}, and $H_2/CO_2/N_2$ = 70/20/10.

The catalytic performance of CO_2 hydrogenation over the Ir/TiO_2-x catalysts was then compared with that of state-of-the-art catalysts. As shown in Table S1,† for the CO_2 methanation reaction, the activity of the Ir/TiO_2-200 catalyst is inferior to that of Ru- and the benchmark Ni-based catalysts since they always exhibit excellent hydrogenation properties. As for the reverse water–gas shift reaction, Ir/TiO_2-700 exhibits an activity comparable to or higher than that of the reported catalysts. Nevertheless, the product selectivity on the Ir/TiO_2 catalysts can be tuned from CH_4 to exclusively CO just by varying the reduction temperature (Fig. 1 and Fig. S1†), which may help uncover the intrinsic factors that govern product selectivity and may offer greener pathways for the conversion of CO_2.

In Fig. 2a, similar slopes of Arrhenius plots for CO_2 conversion are observed, *i.e.*, similar apparent activation energies (E_a) were calculated for CO_2 activation over these Ir/TiO_2-x catalysts. However, the slopes of Arrhenius plots for CH_4 production greatly increased along with the increase of pretreatment temperature from 200 to 700 °C (Fig. 2b). A reverse trend is observed for the variation of E_a for CO production (Fig. S2†). From the calculated data, the E_a values for CH_4 production manifest a significant increase from 39.6 to 233.9 kJ mol^{-1}, while those for CO production appear to exhibit a modest decrease from 50.7 to 41.1 kJ mol^{-1} (Table S2†). Note that the E_a values for CO_2 conversion all lie in a lower value range (40.5–47.1 kJ mol^{-1}), indicative of the facile activation of CO_2 over all Ir/TiO_2-x catalysts. The increased barrier for CH_4 production together with the decreased barrier for CO production offers a great opportunity for modulating the selectivity in the CO_2 hydrogenation process. The tremendous shift of product selectivity together with the corresponding soaring increase of E_a for CH_4 production greatly motivates us to investigate the intrinsic variation of Ir/TiO_2-x catalysts as the pretreatment temperature varies.

Structure identification of Ir/TiO_2-x catalysts

The structure variations with the increasing pretreatment temperature of Ir/TiO_2 catalysts were first studied by a set of characterization techniques. As shown in Fig. S3 and Table S3,† these Ir/TiO_2-x catalysts possess similar BET surface areas and pore volumes. From XRD patterns, there is no characteristic peak for metallic Ir or IrO_2 phases for all Ir/TiO_2-x catalysts (Fig. S4†), indicative of a high dispersion of Ir

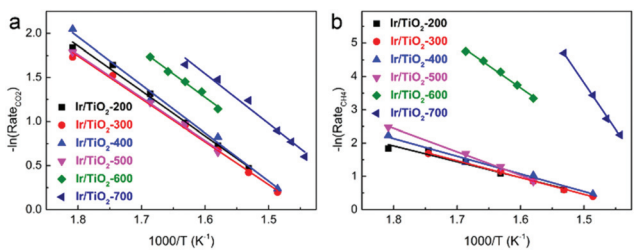

Fig. 2 Arrhenius plots for (a) CO_2 conversion and (b) CH_4 production over Ir/TiO_2-x catalysts.

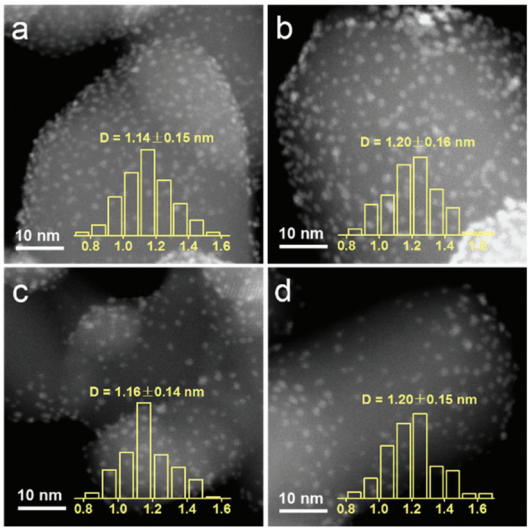

Fig. 3 HAADF-STEM images of the series Ir/TiO_2-*x* catalysts with the metal size distribution. (a) Ir/TiO_2-200; (b) Ir/TiO_2-400; (c) Ir/TiO_2-600; and (d) Ir/TiO_2-700.

species on the rutile TiO_2 support. As observed from the HAADF-STEM images in Fig. 3, Ir nanoparticles in all these Ir/TiO_2-*x* catalysts are highly dispersed and manifest a uniform size distribution with a diameter of 1.1–1.2 nm. The good stability of Ir NPs was primarily due to the employment of rutile TiO_2, which possesses similar lattice parameters with those of rutile IrO_2 (Table S4†). Upon calcination in air, IrO_2 tends to spread onto TiO_2 and facilely forms an $Ir_xTi_{1-x}O_2$ interphase between surface IrO_2 and the TiO_2 substrate (IrO_2/$Ir_xTi_{1-x}O_2$/TiO_2), which in turn resists the aggregation of Ir NPs even after a pretreatment at a temperature of 700 °C.

The reduction behavior of the as-prepared Ir/TiO_2 catalyst was then acquired by a H_2-TPR experiment. As shown in Fig. 4, two main reduction peaks (at 83 and 184 °C) are observed before 300 °C, which are attributed to the reduction of surface IrO_2 and Ir species in the $Ir_xTi_{1-x}O_2$ interphase, respectively. The H_2 consumption for the two stages (between 50–285 °C) was measured as 253.7 μmol g^{-1}, which is approximately equivalent to the theoretical estimation of 254.9 μmol g^{-1} for IrO_2 reduction (Table S5†). The total H_2 consumption is 1.58 times that of theoretical estimation for full reduction of the IrO_2 phase, indicative of the co-reduction of TiO_2 in the Ir/TiO_2 catalyst, which can be confirmed by the broad peaks at 320 and 530 °C. Benefiting from the formation of the $Ir_xTi_{1-x}O_2$ interphase, the reduction of TiO_2 in Ir/TiO_2 is greatly facilitated[29] in comparison with that of pure TiO_2 (at 671 °C) due to the facile hydrogen spillover. Therefore, for the Ir/TiO_2 catalysts pretreated at temperatures less than 300 °C, *i.e.*, the Ir/TiO_2-200 and Ir/TiO_2-300 samples, there are predominantly exposed metallic Ir NPs on the surface of TiO_2 support. For the Ir/TiO_2 catalysts pretreated at temperatures higher than 300 °C, apart from the reduction of IrO_2, there is also co-reduction of TiO_2. Accordingly, the degree of reduction of Ir/TiO_2 was supposed to be improved with the increase of pretreatment temperature.

As reported previously, the chemical state of Ir species plays a vital role in tuning the selectivity of CO_2 hydrogenation, that is, metallic Ir NPs preferred CH_4 production while partially oxidized Ir species favored CO production.[22] In our case, the chemical states of Ir/TiO_2-*x* catalysts were then investigated with X-ray photoelectron spectroscopy (XPS). As shown in Fig. 5a, the peaks approximately at 60.5 eV (Ir $4f_{7/2}$) and 63.3 eV (Ir $4f_{5/2}$) are attributed to metallic Ir species.[30,31] In the Ir/TiO_2-200 sample, both metallic Ir^0 and partially oxidized $Ir^{\delta+}$ species contribute to the observed binding energies of 61.4 eV (Ir $4f_{7/2}$) and 64.0 eV (Ir $4f_{5/2}$), which is due to the incomplete reduction of Ir NPs as confirmed by H_2-TPR results. The shift in binding energy from 61.4 to 60.2 eV with the increase of reduction temperature suggests a gradual improvement of the degree of reduction of Ir NPs. Combined with the reaction data above, the improved degree of reduction failed to promote CH_4 production, indicating that the chemical state of Ir species may not be the decisive factor on product selectivity. It thus motivates us to focus on other discrepancies originating from the variation of micro-structures in Ir/TiO_2 influenced by different reduction treatments.

As previously reported by Tauster *et al.*,[26–28] there are strong metal–support interactions (SMSI) over TiO_2 supported Ir cata-

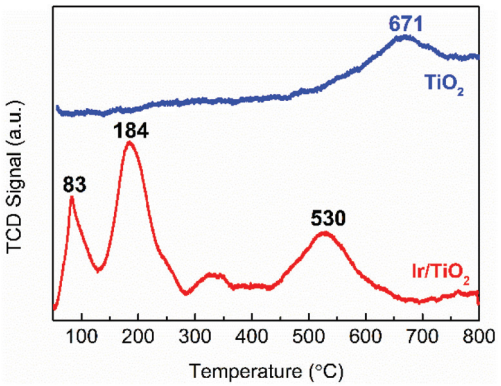

Fig. 4 H_2-TPR profiles of the Ir/TiO_2 catalyst and the TiO_2 support.

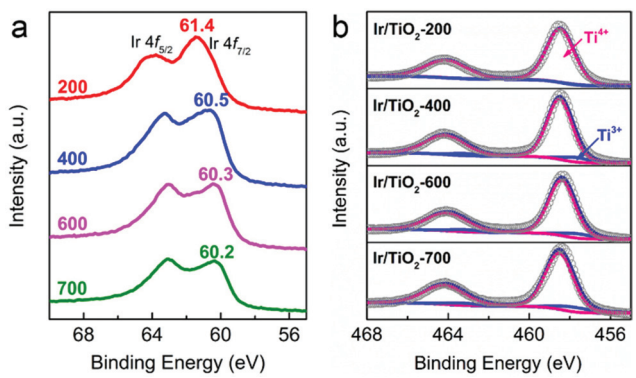

Fig. 5 (a) Ir 4f and (b) Ti 2p XP spectra of Ir/TiO_2-*x* catalysts.

lysts, in which reduced TiO_x species migrates onto the metal surfaces and further forms a coating on the metal particles. Consequently, the chemisorption of CO and H_2 can be severely suppressed, which usually alters the catalytic performance of CO_2 hydrogenation. As indicated by the Ti 2p XP spectra (Fig. 5b and Table S6†), the increased Ti^{3+} concentration (from 1.1% to 9.7%) might be a reflection of the enhanced TiO_x coating over Ir NPs when the pretreatment temperature was varied from 200 to 700 °C.

HRTEM observations provide intuitive information about the discrepancies in micro-structures with varying reduction temperature. As shown in Fig. 6, the Ir/TiO_2-200 sample shows angular particles on the TiO_2 support with a clear boundary due to a dominant reduction of IrO_2 to metallic Ir, while an increased coating over Ir NPs is distinguishable with the pre-reduction temperature varying from 400 to 700 °C. This phenomenon is ascribed to a gradual migration of TiO_x overlayer to the Ir NPs. Furthermore, CO was used as a probe in detecting the *in situ* diffuse reflectance infrared Fourier transform (DRIFT) spectra, with the aim of getting a qualitative comparison of the degree of exposure of Ir NPs after coating by TiO_x overlayer. The main band appeared at 2080–2040 cm^{-1} in the carbonyl region (Fig. 7), which was attributed to the linear CO adsorption on Ir NPs.[32] An obvious decay of the DRIFT intensity was observed as the pretreatment temperature varied from 300 to 700 °C, indicative of a reduced Ir exposure, which in turn demonstrated the growth of TiO_x coating on Ir NPs. The intensity of CO adsorption on the Ir/TiO_2-200 sample was found to be a little less than that of Ir/TiO_2-300 probably due to the lower degree of reduction of Ir species in Ir/TiO_2-200.

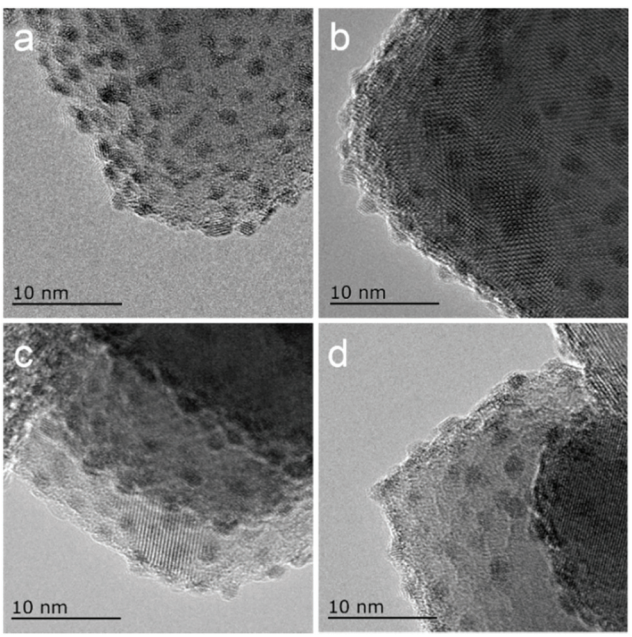

Fig. 6 HRTEM images of the series of Ir/TiO_2-*x* catalysts. (a) Ir/TiO_2-200; (b) Ir/TiO_2-400; (c) Ir/TiO_2-600; and (d) Ir/TiO_2-700.

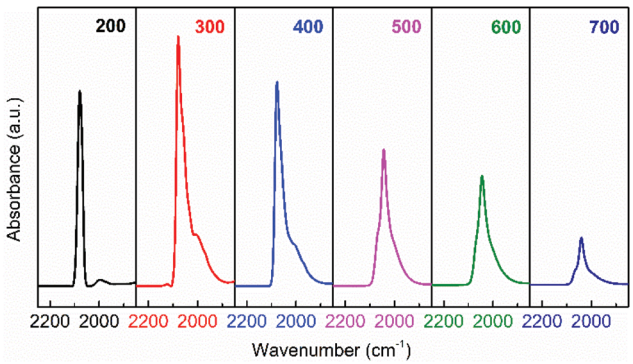

Fig. 7 *In situ* DRIFT spectra obtained after CO adsorption and evacuation with helium at room temperature (25 °C), over the series of Ir/TiO_2-*x* catalysts.

H_2 and CO chemisorption experiments were further conducted to estimate the dispersion of Ir species on Ir/TiO_2-*x* catalysts. As shown in Table 1, the values determined by both H_2 and CO probe molecules indicate the same tendency for different Ir/TiO_2-*x* samples, that is, the dispersion of Ir decreases with the increase of reduction temperature from 300 to 700 °C. Ir/TiO_2 catalysts pretreated at temperatures higher than 600 °C even lost their H_2 or CO adsorption ability, which suggests an almost complete encapsulation of Ir NPs by the TiO_x overlayer. Meanwhile, both H_2 and CO uptakes on the Ir/TiO_2-200 catalyst were found to be less than those on Ir/TiO_2-300, primarily due to the insufficient reduction of Ir/TiO_2-200, as indicated by H_2-TPR and XPS results. The variation in Ir dispersion conforms with the results of HRTEM observations and DRIFT spectra and might be the most likely reason for the selectivity change in CO_2 hydrogenation as all these Ir/TiO_2-*x* catalysts manifest an analogous size distribution.

Structure evolution and the proposed catalytic mechanism of Ir/TiO_2-*x* catalysts

On the basis of the above observations, a structure evolution of Ir/TiO_2 catalysts at different reduction stages is then proposed (Fig. 8). Benefiting from the similar lattice parameters between IrO_2 and rutile TiO_2, highly dispersed Ir/TiO_2 catalysts with a desired sintering resistance and similar particle size can be facilely fabricated. By varying the reduction temperature, the strong metal–support interaction in Ir/TiO_2-*x* can be modu-

Table 1 H_2 and CO chemisorption results for the series of Ir/TiO_2-*x* catalysts

Sample	H_2 uptake ($\mu mol\ g_{Ir}^{-1}$)	D_{Ir} by H_2	CO uptake ($\mu mol\ g_{Ir}^{-1}$)	D_{Ir} by CO
Ir/TiO_2-200	33.6	52.8%	63.8	50.1%
Ir/TiO_2-300	36.4	57.2%	69.4	54.5%
Ir/TiO_2-400	24.0	37.7%	50.2	39.4%
Ir/TiO_2-500	3.59	5.63%	6.94	5.45%
Ir/TiO_2-600	2.18	3.42%	4.39	3.44%
Ir/TiO_2-700	0.12	0.20%	0.29	0.22%

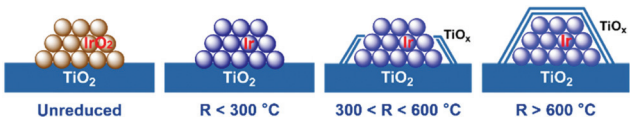

Fig. 8 A schematic illustration of the structural evolution of Ir/TiO_2-*x* catalysts. The gradually brighter color on Ir species suggests an improvement of the degree of reduction for Ir NPs.

lated accordingly, where a TiO_x overlayer gradually appears and migrates on to Ir NPs, resulting in a shrinkage of the metallic Ir surface. The formation of TiO_x coating by SMSI plays an important role in the selectivity change. For the Ir/TiO_2-*x* catalysts treated at lower temperatures (x < 300 °C), there are dominant metallic Ir NPs, on which CO_2 methanation can be facilitated as reported in our previous study.[21] As for the samples treated with a moderate reduction (300 < x < 600 °C), the TiO_x overlayer begins to migrate and coat the Ir surface and results in a shrinkage of the metallic Ir surface. In combination with the partially exposed Ir surfaces and a TiO_x thin layer, both CO_2 methanation and reverse water–gas shift (RWGS) processes will happen on the Ir/TiO_2-*x* catalysts. With the increase of TiO_x coating, the RWGS process producing CO is promoted accordingly. On the contrary, for the samples treated with an excessive reduction (x > 600 °C), Ir NPs are entirely encapsulated with the TiO_x overlayer. The RWGS process on TiO_x coating is facile to realize, while further hydrogenation to produce CH_4 is completely suppressed due to the unreachable Ir surfaces.

Considering the structural evolution in relation to the corresponding catalytic performance, CO probably serves as the intermediate during CO_2 methanation over Ir/TiO_2-*x* catalysts. As all these Ir/TiO_2-*x* catalysts manifest similar reaction rates and E_a for CO_2 conversion with a low value of ~45 kJ mol^{-1}, it is facile to realize CO_2 activation. An increased barrier for CH_4 production is observed as the reduction temperature increases, during which the encapsulation of Ir NPs results in an enhanced RWGS process to produce CO. When the reduction temperature is increased to modulate the metal-support interaction, the TiO_x thin layer gradually migrates on to the surface of Ir NPs, which plays a vital role in further transformation of product selectivity from CH_4 to CO.

Experimental

Catalyst preparation

Ir/TiO_2 catalysts were prepared *via* a wetness impregnation method. In a typical synthesis, 0.42 g of the H_2IrCl_6 solution (38 wt%, 0.1418 g Ir per gram of solution, AR) was diluted to 50 mL with deionized water. Following this, 2.0 g of rutile TiO_2 was added to the solution and the resulting suspension was dried in a 50 °C water bath with vigorous stirring through evaporation. The resulting solid was dried at 120 °C for 12 h, followed by calcination in air at 400 °C for 4 h. In order to remove the residual chlorides, the sample was then washed repeatedly with a dilute ammonia solution (1 mol L^{-1}), followed by filtration and drying at 80 °C overnight. The sample thus obtained was denoted as the fresh Ir/TiO_2 catalyst. The loading of Ir on the Ir/TiO_2 catalyst was 2.45 wt% as detected by ICP. Prior to CO_2 hydrogenation tests, the as-prepared Ir/TiO_2 sample was reduced *in situ* in a H_2 flow (20 mL min^{-1}) at specific temperatures, denoting them as Ir/TiO_2-*x*, where *x* indicates the reduction temperature (200, 300, 400, 500, 600 or 700 °C).

Catalyst characterization

Powder X-ray diffraction (XRD) data were acquired using a PANalytical X'Pert-Pro X-ray diffractometer operated at 40 kV and 40 mA. Nitrogen physisorption was performed with a Micromeritics ASAP 2460 instrument at −196 °C. TEM observations, including high-angle annular dark field scanning transmission electron microscopy (HAADF-STEM) and high-resolution transmission electron microscopy (HRTEM) images, were acquired using a JEOL JEM-2100F microscope operated at 200 kV. The Ir concentration in the Ir/TiO_2 catalyst was determined by inductively coupled plasma optical emission spectroscopy (ICP-OES) with an ICP-OES 7300DV instrument.

H_2 temperature programmed reduction (H_2-TPR) was performed with a Micromeritics AutoChem II 2920 apparatus. Prior to TPR measurement, the pristine Ir/TiO_2 sample was pretreated with Ar at 200 °C for 60 min. After the temperature was reduced to 50 °C, a 10% H_2/Ar flow was introduced into the reactor by heating the sample to 800 °C at a heating rate of 10 °C min^{-1}. The signal was recorded online with a thermal conductivity detector (TCD).

X-ray photoelectron spectroscopy (XPS) data were obtained using a Thermo Fisher ESCALAB 250Xi instrument, employing monochromated Al Kα radiation ($h\upsilon$ = 1486.6 eV) as the X-ray source. The sample was pretreated at the desired temperature in a H_2 flow and then held under an inert atmosphere, followed by rapid transfer to the sample chamber to minimize exposure to air. The results were calibrated by setting the C 1s adventitious carbon peak position to 284.6 eV.

In situ diffuse reflectance infrared Fourier transform (DRIFT) spectra were acquired using a Bruker Equinox 55 spectrometer recorded with a resolution of 4 cm^{-1}. The sample was treated *in situ* under a H_2 flow (20 mL min^{-1}) at the desired temperature for 60 min. After cooling to room temperature (25 °C), the gas flow was purged with He for 30 min, following which the background spectrum was collected. Then, the He flow was switched to a 5 vol% CO in He flow (20 mL min^{-1}) which was maintained until saturated adsorption was achieved. The system was purged with He to remove non-adsorbed CO and DRIFT spectra were collected, such that CO adsorption data at room temperature were obtained.

The exposure of Ir NPs was determined by CO and H_2 chemisorption on a Micromeritics AutoChem II 2920 instrument. For the CO (or H_2) chemisorption experiment, the sample was pretreated in a H_2 flow at the desired temperature for 60 min, followed by purging with He (or Ar) for 30 min. After cooling

down to 50 °C, a 5% CO in He (or 10% H_2 in Ar) was injected into the reactor repeatedly until saturated adsorption is achieved. The dispersion of Ir was determined by assuming the CO/Ru (or H/Ru) adsorption stoichiometry to be 1:1.

Catalyst testing

CO_2 hydrogenation reactions were performed in a fixed-bed quartz reactor at atmospheric pressure. Prior to each reaction, the Ir/TiO_2 catalyst (0.15 g) was *in situ* reduced in a H_2 flow (20 mL min^{-1}) at the desired temperature for 2 h. After the reactor was cooled down, a feed gas with a H_2/CO_2 ratio of 3.5/1 ($H_2/CO_2/N_2$ = 70/20/10 (v/v/v), N_2 was used as an internal standard) was introduced into the reactor for CO_2 hydrogenation tests. The reactions were carried out at 280 °C and 9000 mL g_{cat}^{-1} h^{-1}. After passing through an ice bath, the gaseous products were analyzed online using an A90 Echrom gas chromatograph equipped with a TDX-01 column connected to a thermal conductivity detector (TCD).

The CO_2 conversion, X_{CO_2}, was calculated using the following equation:

$$X_{CO_2} = \frac{n_{in}(CO_2) - n_{out}(CO_2)}{n_{in}(CO_2)} = 1 - \frac{A_{out}(CO_2)/A_{out}(N_2)}{A_{in}(CO_2)/A_{in}(N_2)},$$

where $n_{in}(CO_2)$ and $n_{out}(CO_2)$ refer to the mole number of CO_2 at the inlet and outlet, respectively; $A_{in}(CO_2)$ and $A_{in}(N_2)$ refer to the chromatographic peak areas of CO_2 and N_2 in the feed gas; and $A_{out}(CO_2)$ and $A_{out}(N_2)$ refer to the chromatographic peak areas of CO_2 and N_2 in the off-gas.

The reaction rate was calculated as:

$$\text{Reaction rate} = \frac{\text{GHSV} \times X_{CO_2} \times \text{CO}_2 \text{ concentration}}{22\,400 \times \omega_{Ir}},$$

where GHSV is the gas hourly space velocity and ω_{Ir} is the mass fraction of Ir (2.45 wt% as detected by ICP-OES).

For the off-gas consisting only of CO (or CH_4), the selectivity toward CO (or CH_4) was assumed to be 100%. For the products in the off-gas consisting of both CO and CH_4, the selectivity values for CO and CH_4 (S_{CO} and S_{CH_4}) were acquired by a normalization method:

$$S_{CO} + S_{CH_4} = 1,$$

$$S_{CO} = f_{CO/CH_4} \times \frac{A_{CO}}{A_{CH_4}} \times S_{CH_4},$$

where f_{CO/CH_4} is the relative correction factor of CO to CH_4, which was determined by the calibrating gas; and A_{CO} and A_{CH_4} refer to the chromatographic peak areas of CO and CH_4, respectively.

Conclusions

In conclusion, we have successfully fabricated a series of highly dispersed, similar sized Ir/TiO_2 catalysts with sintering resistance to high temperature treatment. By varying the reduction temperature to modulate the metal–support interaction, the product selectivity of catalytic CO_2 hydrogenation can be tuned from CH_4 to CO. The reduced TiO_x species that originated from SMSI plays a crucial role in tuning the product selectivity. Ir NPs encapsulated with a TiO_x coating show a preference for CO production with an inhibition of further hydrogenation, while exposed Ir NPs without TiO_x promote CH_4 production exclusively. This study provides an understanding of the regulation of CO_2 hydrogenation by SMSI and can serve as an effective approach to tailoring other catalytic processes.

Conflicts of interest

There are no conflicts to declare.

Acknowledgements

This work was supported by the National Key R&D Program of China (2016YFA0202804), the Strategic Priority Research Program of the Chinese Academy of Sciences (XDB36030200), the National Natural Science Foundation of China (21978286, 21925803, 21776269), and the Youth Innovation Promotion Association CAS.

Notes and references

1 X. Wang, H. Shi and J. Szanyi, *Nat. Commun.*, 2017, **8**, 513–518.
2 X. Jia, K. Sun, J. Wang, C. Shen and C.-J. Liu, *J. Energy Chem.*, 2020, **50**, 409–415.
3 L. Wang, E. Guan, Y. Wang, L. Wang, Z. Gong, Y. Cui, X. Meng, B. C. Gates and F. S. Xiao, *Nat. Commun.*, 2020, **11**, 1033–1041.
4 A. Modak, P. Bhanja, S. Dutta, B. Chowdhury and A. Bhaumik, *Green Chem.*, 2020, **22**, 4002–4033.
5 B. An, Z. Li, Y. Song, J. Zhang, L. Zeng, C. Wang and W. Lin, *Nat. Catal.*, 2019, **2**, 709–717.
6 J. Zhu, G. Zhang, W. Li, X. Zhang, F. Ding, C. Song and X. Guo, *ACS Catal.*, 2020, **10**, 7424–7433.
7 F. Wang, C. Li, X. Zhang, M. Wei, D. G. Evans and X. Duan, *J. Catal.*, 2015, **329**, 177–186.
8 K. Wang, W. Li, J. Huang, J. Huang, G. Zhan and Q. Li, *J. Energy Chem.*, 2021, **53**, 9–19.
9 J. Gödde, M. Merko, W. Xia and M. Muhler, *J. Energy Chem.*, 2021, **54**, 323–331.
10 M. D. Porosoff, S. Kattel, W. Li, P. Liu and J. G. Chen, *Chem. Commun.*, 2015, **51**, 6988–6991.
11 Y. Ma, Z. Guo, Q. Jiang, K.-H. Wu, H. Gong and Y. Liu, *J. Energy Chem.*, 2020, **50**, 37–43.
12 R. Carrasquillo-Flores, I. Ro, M. D. Kumbhalkar, S. Burt, C. A. Carrero, A. C. Alba-Rubio, J. T. Miller, I. Hermans, G. W. Huber and J. A. Dumesic, *J. Am. Chem. Soc.*, 2015, **137**, 10317–10325.

13 A. Karelovic and P. Ruiz, *Appl. Catal., B*, 2012, **113–114**, 237–249.
14 J. H. Kwak, L. Kovarik and J. Szanyi, *ACS Catal.*, 2013, **3**, 2449–2455.
15 A. Aitbekova, L. Wu, C. J. Wrasman, A. Boubnov, A. S. Hoffman, E. D. Goodman, S. R. Bare and M. Cargnello, *J. Am. Chem. Soc.*, 2018, **140**, 13736–13745.
16 S. Kattel, W. Yu, X. Yang, B. Yan, Y. Huang, W. Wan, P. Liu and J. G. Chen, *Angew. Chem., Int. Ed.*, 2016, **55**, 7968–7973.
17 J. H. Kwak, L. Kovarik and J. Szanyi, *ACS Catal.*, 2013, **3**, 2094–2100.
18 W. Li, G. Zhang, X. Jiang, Y. Liu, J. Zhu, F. Ding, Z. Liu, X. Guo and C. Song, *ACS Catal.*, 2019, **9**, 2739–2751.
19 M. D. Porosoff and J. G. Chen, *J. Catal.*, 2013, **301**, 30–37.
20 J. C. Matsubu, V. N. Yang and P. Christopher, *J. Am. Chem. Soc.*, 2015, **137**, 3076–3084.
21 X. Chen, X. Su, H.-Y. Su, X. Liu, S. Miao, Y. Zhao, K. Sun, Y. Huang and T. Zhang, *ACS Catal.*, 2017, **7**, 4613–4620.
22 S. Li, Y. Xu, Y. Chen, W. Li, L. Lin, M. Li, Y. Deng, X. Wang, B. Ge, C. Yang, S. Yao, J. Xie, Y. Li, X. Liu and D. Ma, *Angew. Chem., Int. Ed.*, 2017, **56**, 10761–10765.
23 F. Wang, S. He, H. Chen, B. Wang, L. Zheng, M. Wei, D. G. Evans and X. Duan, *J. Am. Chem. Soc.*, 2016, **138**, 6298–6305.
24 J. Xu, X. Su, H. Duan, B. Hou, Q. Lin, X. Liu, X. Pan, G. Pei, H. Geng, Y. Huang and T. Zhang, *J. Catal.*, 2016, **333**, 227–237.
25 S. Li, G. Liu, S. Zhang, K. An, Z. Ma, L. Wang and Y. Liu, *J. Energy Chem.*, 2020, **43**, 155–164.
26 S. J. Tauster, S. C. Fung, R. T. K. Baker and J. A. Horsley, *Science*, 1981, **211**, 1121–1125.
27 S. J. Tauster, *Acc. Chem. Res.*, 1987, **20**, 389–394.
28 S. J. Tauster, S. C. Fung and R. L. Garten, *J. Am. Chem. Soc.*, 1978, **100**, 170–175.
29 A. Gómez-Cortés, G. Díaz, R. Zanella, H. Ramírez, P. Santiago and J. M. Saniger, *J. Phys. Chem. C*, 2009, **113**, 9710–9720.
30 H. N. Nong, L. Gan, E. Willinger, D. Teschner and P. Strasser, *Chem. Sci.*, 2014, **5**, 2955–2963.
31 R. Jin, M. Peng, A. Li, Y. Deng, Z. Jia, F. Huang, Y. Ling, F. Yang, H. Fu, J. Xie, X. Han, D. Xiao, Z. Jiang, H. Liu and D. Ma, *J. Am. Chem. Soc.*, 2019, **141**, 18921–18925.
32 F. Solymosi, E. Novak and A. Molnar, *J. Phys. Chem.*, 1990, **94**, 7250–7255.